

# JGR Biogeosciences

## RESEARCH ARTICLE

10.1029/2019JG005445

### Key Points:

- Tree ring mercury levels in Shenandoah National Park, Virginia, were similar to those measured in other North American forests
- Tree ring mercury peaked during the 1930s to 1950s, coinciding with mercury use at an industrial facility near the southern end of the Park
- Mercury isotopes suggest a local source at this time, demonstrating the potential of dendrochemistry to identify historical sources

### Supporting Information:

- Supporting Information S1

### Correspondence to:

T. M. Scanlon,  
tms2v@virginia.edu

### Citation:

Scanlon, T. M., Riscassi, A. L., Demers, J. D., Camper, T. D., Lee, T. R., & Druckenbrod, D. L. (2020). Mercury accumulation in tree rings: Observed trends in quantity and isotopic composition in Shenandoah National Park, Virginia. *Journal of Geophysical Research: Biogeosciences*, 125, e2019JG005445. <https://doi.org/10.1029/2019JG005445>

Received 27 AUG 2019

Accepted 10 JAN 2020

Accepted article online 16 JAN 2020

### Author Contributions:

**Conceptualization:** T. M. Scanlon, A. L. Riscassi, D. L. Druckenbrod  
**Data curation:** T. M. Scanlon, D. L. Druckenbrod  
**Formal analysis:** T. M. Scanlon, A. L. Riscassi, J. D. Demers, T. R. Lee, D. L. Druckenbrod  
**Funding acquisition:** T. M. Scanlon  
**Investigation:** T. M. Scanlon, A. L. Riscassi, J. D. Demers, T. D. Camper, D. L. Druckenbrod  
**Methodology:** T. M. Scanlon, A. L. Riscassi, J. D. Demers, T. D. Camper, T. R. Lee, D. L. Druckenbrod  
**Project administration:** T. M. Scanlon, A. L. Riscassi  
**Resources:** T. M. Scanlon  
*(continued)*

©2020. American Geophysical Union.  
All Rights Reserved.

## Mercury Accumulation in Tree Rings: Observed Trends in Quantity and Isotopic Composition in Shenandoah National Park, Virginia

T. M. Scanlon<sup>1</sup> , A. L. Riscassi<sup>1</sup> , J. D. Demers<sup>2</sup> , T. D. Camper<sup>1,3</sup> , T. R. Lee<sup>4,5</sup> , and D. L. Druckenbrod<sup>6</sup> 

<sup>1</sup>Department of Environmental Sciences, University of Virginia, Charlottesville, VA, USA, <sup>2</sup>Department of Earth and Environmental Sciences, University of Michigan, Ann Arbor, MI, USA, <sup>3</sup>Now at U.S. Geological Survey, Virginia Water Science Center, Richmond, VA, USA, <sup>4</sup>Cooperative Institute for Mesoscale Meteorological Studies (CIMMS), Norman, OK, USA, <sup>5</sup>NOAA Air Resources Laboratory Atmospheric Turbulence and Diffusion Division, Oak Ridge, TN, USA,

<sup>6</sup>Department of Geological, Environmental, and Marine Sciences, Rider University, Lawrenceville, NJ, USA

**Abstract** Recent studies have shown that mercury (Hg) concentrations in tree rings have the potential to archive historical Hg exposure from local, regional, and global sources. The southeastern United States has received elevated Hg deposition, yet no studies have evaluated tree ring Hg in this region. Here, we quantify Hg accumulation and isotopic composition in tree rings collected in Shenandoah National Park, Virginia. Cores were collected from three individuals of three tree species—white oak (*Quercus alba*), northern red oak (*Quercus rubra*), and pitch pine (*Pinus rigida*)—within the northern, central, and southern areas of the Park ( $n = 27$  cores). The cores were analyzed for Hg content in 10-year increments, with some cores dating back to the early 1800s. Overall, tree ring Hg concentrations (ranging from below detection to 4.4 ng/g) were similar to other studies and varied between species, with pitch pine having higher concentrations than the deciduous species. The most notable feature of the tree ring Hg time series was a peak that occurred during the 1930s through 1950s, coinciding with the use of Hg at a local industrial facility. Atmospheric modeling indicates that potential emissions from the plant likely had a stronger impact on the southern region of the Park, consistent with the latitudinal gradient in tree ring Hg concentrations. Mass-dependent and mass-independent fractionation of Hg isotopes suggests contributions from both regional anthropogenic and local industrial sources during this period. This study demonstrates the potential usefulness of tree ring dendrochemistry for identifying historical sources of atmospheric Hg exposure.

**Plain Language Summary** For many years scientists have used tree rings to reconstruct past climate. Increasingly, tree rings are being used to document the historical exposure of trees to pollutants. In this study, we cored trees in Shenandoah National Park, Virginia, dated the tree rings, and then measured the amount of mercury stored within decadal core increments. We were surprised to find that mercury levels peaked in the 1930s to 1950s, even though global mercury emissions continued to rise throughout the past century, mostly as a by-product of energy production. Our findings suggest that the trees were exposed to a local pollutant source during this earlier time period, perhaps from a nearby industrial plant that used mercury in the production of rayon. By examining the chemistry of wood within tree rings, we can get a clearer picture of when and where human activities have affected air pollution over recent centuries.

## 1. Introduction

Mercury (Hg) is a pollutant that is highly mobile in the atmosphere, persistent in the environment, and toxic to both wildlife and humans. Presently, the main source of Hg to the atmosphere is the reemission of previously deposited Hg found in soils, vegetation, and surface waters, originating from both natural geogenic and anthropogenic sources (Pacyna et al., 2016; UNEP, 2013). Although historical Hg emissions and subsequent deposition play a dominant role in shaping current and future Hg cycling, our knowledge of Hg levels in the environment prior to the 21st century is relatively limited in both space and time. Here, we investigate historical accumulation of Hg in trees in Shenandoah National Park, Virginia, a location downwind from coal combustion sources that have impacted air quality throughout the eastern United States since the time of the Industrial Revolution.

**Software:** T. M. Scanlon, A. L. Riscassi, J. D. Demers

**Supervision:** T. M. Scanlon

**Visualization:** T. M. Scanlon, A. L. Riscassi, J. D. Demers

**Writing - original draft:** T. M. Scanlon, A. L. Riscassi, T. D. Camper

**Writing - review & editing:** T. M. Scanlon, A. L. Riscassi, J. D. Demers, T. D. Camper, T. R. Lee, D. L. Druckenbrod

Our current understanding of historical Hg deposition and accumulation is derived from a variety of natural environmental archives that include ice (Beal et al., 2015; Chellman et al., 2017; Schuster et al., 2002), lake bottom sediment (Drevnick et al., 2012, and references therein), and peat cores (Biester et al., 2007, and references therein). Studies conducted in remote locations have been used to estimate “global” atmospheric Hg levels (Chellman et al., 2017; Colman et al., 1999; Heyvaert et al., 2000; Lamborg et al., 2002; Landers et al., 2010; Schuster et al., 2002; Yake, 2001); both ice cores and lake sediments indicate an approximately threefold to fivefold increase in the Northern Hemisphere since the start of industrialization in the late 1800s. Sediment cores have also documented regional atmospheric Hg signals in the Great Lakes region (Pirrone et al., 1998) and from major fires and volcanic eruptions (Daga et al., 2016). An emerging approach to reconstruct trends in atmospheric Hg is through the use of dendrochemistry (Clackett et al., 2018; Navratil et al., 2018; Peckham et al., 2019; Wright et al., 2014). With careful sampling strategies, tree cores may provide a regionally integrated atmospheric Hg archive while avoiding problems associated with other methods, such as uncertain geochemical dating of peat (Biester et al., 2007) and diagenetic remobilization in sediments (Sunderland et al., 2008).

Trace metals become incorporated into woody tissues by three potential pathways: (1) via roots from soil/groundwater, (2) via foliar translocation, or (3) via absorption through bark into the cambial layer from the atmosphere (Odabasi et al., 2016). A recent experimental study by Arnold et al. (2018) found that of these three potential pathways, foliar uptake (via both stomata and cuticles) and subsequent translocation by way of phloem were the only ones that led to substantial accumulation of Hg in the tree woody tissue. Therefore, tree ring Hg is thought to be most closely associated with ambient levels of gaseous elemental mercury, since gaseous elemental mercury is the predominant form of Hg taken up by foliage (Peckham et al., 2019; Rutter et al., 2011). Radial translocation can have the effect of smearing or otherwise altering Hg time series captured by tree rings (Arnold et al., 2018), but the observed correspondence between tree ring Hg anomalies and the timing of local industrial activities (Navratil et al., 2018) and the fact that disparate-aged trees appear to agree on the chronological timing of Hg anomalies (Clackett et al., 2018) provide evidence that translocation may not be significant, at least for the species studied (European larch in Navratil et al., 2018 and white spruce in Clackett et al., 2018).

Tree rings collected from a remote forest stand in northwestern Canada exhibited a long-term rise in Hg concentrations from 1750 to the present (Clackett et al., 2018), consistent with modeled trends in global-scale Hg concentrations (Horowitz et al., 2014). In the western United States, there was some evidence of industrialization era increases in tree ring Hg, along with indications of a regional atmospheric Hg source (i.e., the California Gold Rush) from several trees (Wright et al., 2014). Meanwhile, other studies have focused on the impact from local sources, looking at differences in tree core Hg concentrations between contaminated and reference sites (Siwik et al., 2010) and variations with distance from industrial plants (Jung & Ahn, 2017; Navratil et al., 2017). Temporal correlations have been documented between tree core Hg concentrations and trends in anthropogenic emissions based on the number of industries in a region of Turkey (Odabasi et al., 2016), production from a local metal smelter in the Czech Republic (Hojdová et al., 2011), and chlorine production rates at a site in France (Maillard et al., 2016). These previous studies suggest that tree ring Hg concentrations have the potential to archive historical atmospheric Hg exposure from sources at the global, regional, and local scales.

In the United States, modeling studies have indicated that total Hg deposition is elevated in the Central Appalachians Mountains (Butler et al., 2007; Corbitt et al., 2011; Gbor et al., 2007), downwind from the concentration of coal-fired power plants located in the Ohio River Valley. Bituminous coal production in the United States, which occurs primarily in the Appalachian Mountains and Midwestern states and is therefore used as a proxy for regional production, increased steadily from 1880 to 1920 and has since remained elevated. To date, no studies have evaluated historical Hg exposure through the analysis of sediment cores or tree rings in this region, despite this being an area of potentially high atmospheric deposition from regional coal combustion that has been active since the late 1800s.

In the current study, our goals are (1) to chronicle the Hg accumulation in tree rings in Shenandoah National Park, Virginia, (2) to determine if there are temporal or spatial trends in Hg accumulation, and (3) to evaluate if the observed Hg time series are consistent with exposure to Hg derived from known local to global sources. Our expectation was that the Hg measured in the tree rings would reflect regional trends in coal

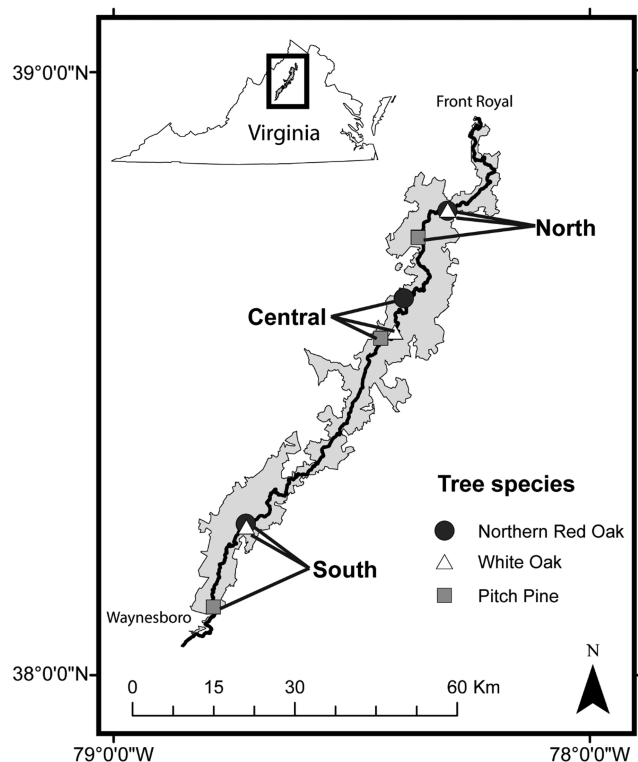


**Figure 1.** Map of tree core sampling sites within the north, central, and southern regions of Shenandoah National Park (SHEN), Virginia. The black line running north to south represents the main road in SHEN, skyline drive, from which sites were accessed.

selection of species was undertaken with the requirement that the targeted species could be found in each of these regions. The following three species were sampled: white oak (*Quercus alba*), northern red oak (*Quercus rubra*), and pitch pine (*Pinus rigida*). Tree coring took place on 4–5 October 2014 along Skyline Drive (Figure 1) in SHEN. In each region of the Park, we collected three cores per tree from three individuals of each tree species (3 locations  $\times$  3 species  $\times$  3 replicate trees  $\times$  3 replicate cores/tree = 81 total cores collected). Of the three replicates that were collected from each tree, one was used for tree ring cross referencing and dating, one was used for total mercury analysis, and one was used for mercury isotopic analysis.

All trees chosen for coring were at least 100 m away from a road and were canopy dominant, relatively long-lived individuals. Tree cores were collected at breast height using either a 16- or 20-in. Haglof® borer with a 0.2-in. (5.15-mm) inner diameter. The borer was cleaned after every coring with 0.5% bromine monochloride (BrCl) solution and wiped dry with a Kimwipe® to remove Hg from the sampling surface and thereby minimize cross contamination between samples. Tree cores for Hg analysis were placed in plastic straws with their ends sealed by Teflon® tape, then sealed in double plastic bags. Cores intended for dendrochronological evaluation were placed in paper straws.

### 2.3. Laboratory Methods

#### 2.3.1. Dendrochronology and Total Mercury Analysis

The set of 27 cores used for dendrochronological analysis was sent to Rider University where they were crossdated, a process that involves the assignment of a calendar year to each ring based on the expression of a common, embedded climate signal affecting growth. Cores were sanded to a final grit using 15- $\mu$ m sandpaper and then measured under a stereomicroscope using a Velmex Tree Ring Measurement Station with 0.001-mm accuracy. Crossdating followed standard methods (Speer, 2010), proceeding with visual crossdating and then statistical verification using the tree ring analysis program COFECHA (Holmes,

combustion, perhaps overlain by similar, long-term trends in global atmospheric Hg concentrations. The results deviated from this expectation, however, leading us to explore the viability of a potential local source. Included in this analysis is the first reported use of Hg isotopes in a dendrochemistry study.

## 2. Methods

### 2.1. Site Description

Shenandoah National Park (SHEN) is located in northwestern Virginia, in the Blue Ridge physiographic province. SHEN is long and narrow, spanning 169 km along the spine of the Blue Ridge Mountains, bookended by the city of Front Royal to the north and the city of Waynesboro to the south (Figure 1). Established in 1935, SHEN covers an area of approximately 800 km<sup>2</sup>, of which 40% is federally designated wilderness. Elevations range from 160 m along the Park perimeter up to a maximum of 1,235 m on the ridge. Overall, SHEN is 95% forested, with oak and oak hickory forests (65%) and cove hardwood forests (13%) as the major components of the landscape (Young et al., 2006). Mercury in biological (Bank et al., 2005; Eagles-Smith et al., 2016), atmospheric (Converse et al., 2010, 2014; Kolker et al., 2008), terrestrial (Gunda & Scanlon, 2013; Risch et al., 2017), and aqueous (Riscassi & Scanlon, 2011, 2013) samples from SHEN has been evaluated, and each of the corresponding studies has indicated that current Hg levels in this ecosystem are within the range measured in natural settings at other U.S. sites.

### 2.2. Sample Collection

Sampling design was constructed to provide representative spatial coverage within the Park, with sites clustered in each of the three Park-designated districts: North, Central, and South (Figure 1). A priori

1983). For white oaks and northern red oaks, we used a white oak reference chronology collected by Dr. Ed Cook in SHEN and held in the International Tree Ring Data Bank (ITRDB; <https://www.ncdc.noaa.gov/paleo-search/study/3012>). The ITRDB did not have a pitch pine reference chronology from SHEN so we used reference chronologies collected from the Virginia piedmont east of SHEN composed of two other species in the same genus: Shortleaf pine and Virginia pine (Druckenbrod et al., 2018). These cross-dated cores were then delivered to the University of Virginia (UVa) to guide the dating of cores used for Hg analysis.

At UVa, the two sets of 27 cores were dried in their straws, cut along the center to increase airflow. This was done on a clean bench under a HEPA filter, following EPA Method 1631, Revision E (U.S. EPA, 2002) guidelines for sample preparation. When dried, the cores were once again double bagged and stored in a cool, dry, dark location. Each core for Hg analysis was counted and marked in 10-year increments independently by two individuals using an Olympus DF PLAN 1.5X microscope under a HEPA filtered and cross referenced with the mounted cores from Rider University. The 10-year increments started in the last full growing season, 2013, and continued backward in time (e.g., 2013–2004, 2003–1994, and 1993–1984). Each core was cut in 10-year increments with a scalpel under the HEPA filter. The scalpel was cleaned between each cutting with a 0.5% BrCl solution and dried with a Kimwipe. The 10-year core segments were placed in clean flasks and weighed. A Teflon sphere was placed on top of the flask to prevent Hg from being introduced from the surrounding air.

The sample preparation (digestion) procedure for oxidation of Hg in tree core segments followed the Appendix to EPA Method 1631 (EPA-821-R-01-013, “Total Mercury in Tissue, Sludge, Sediment, and Soil”). Core segments were digested in 10 ml of a 7:3 ratio HNO<sub>3</sub>/H<sub>2</sub>SO<sub>4</sub> solution overnight and subsequently brought to a simmer over 6 hr the next day, after which the cores were completely digested. Two digestion blanks (only the digestion solution, no core) were included with each batch of 10 core samples and subjected to identical sample processing steps. After the flasks had cooled, the solutions were transferred into Teflon® bottles and the volume was brought up to approximately 50 ml by weight with a 1% BrCl solution; exact weights were recorded for subsequent mass computations. Samples were analyzed using a Tekran 2600 cold-vapor atomic fluorescence spectrophotometer according to procedures defined in the U.S. EPA Method 1631, Revision E (U.S. EPA, 2002). The analytical detection limit was determined to be 0.20 ng/L. The detection limit for each core is dependent on the mass of each 10-year section digested; for all cores, mean weight was 0.22 ( $\pm 0.15$ ) g, corresponding to a mean core detection limit of 0.05 ng/g. Analytical quality assurance was ensured through the use of system and method blanks (evaluated every ~10 samples), matrix spikes, matrix spike duplicates, and a Hg standard solution (evaluated within each analytical run) independent from the one used for the standard curve.

The mean concentration for system and method blanks ( $n = 56$ ) was 0.06 ( $\pm 0.10$ ) ng/L and 0.02 ( $\pm 0.06$ ) ng/L, respectively. The percent recovery for matrix spikes and duplicates ( $n = 55$ ) was 91 ( $\pm 6$ )%. All analytical quality assurance metrics were within guidelines established by the U.S. EPA (2002). Additionally, digestion blanks and a peach leaf Hg standard (~0.20 g of NIST SRN #1547; 31  $\pm$  7 ng/g) were used to determine methodological quality assurance. Digestion blanks consistently had concentrations above the detection limit (mean of 56 digestion blanks = 0.94 ( $\pm 0.83$ ) ng/L; corresponding to the average weight of the core samples (0.22 g), the blank concentration would be equivalent to 0.21 ( $\pm 0.04$ ) ng Hg per g core. As a result, digestion blank concentrations were subtracted from Hg concentrations in the associated batch (two digestion blanks were run for every ~10 samples) to account for the low-level contamination introduced during the digestion process. The average recovery for the peach leaf Hg standards ( $n = 34$ ), used to verify method accuracy, was 90  $\pm$  13%. The mass of Hg in each section of core was calculated by multiplying the measured sample solution concentration (ng/L) by the total volume of the digestion solution (L). The concentration of Hg in the core section was then calculated by dividing the mass of Hg in the core section (ng) by the core section mass (g).

### 2.3.2. Mercury Isotopic Analysis

Tree core segments were aggregated to provide adequate Hg mass for isotope analysis. Guided by the Hg mass and concentration results, the period of record was divided into three time frames to investigate the influence of local industrial and broader regional anthropogenic Hg emissions on observed tree ring Hg accumulation patterns: pre-1929, 1929–1950 (encompassing the known years of Hg use at the DuPont factory in Waynesboro, Virginia), and 1951–2014 (encompassing the modern era).

Sample Hg extraction and preconcentration methods for isotopic analysis are detailed within the supporting information (Text S1). In brief, bole wood Hg was extracted by two-stage combustion with inline trapping of released Hg in order to minimize matrix interferences and concentrate Hg for isotope analysis (Demers et al., 2013). Off-line combustion performance was monitored with procedural blanks and by percent recovery of reference materials. Average procedural blanks were 0.004 ng/g Hg ( $\pm 0.001$  ng/g, 1SD,  $n = 4$ ), representing 1.6% ( $\pm 0.5\%$ , 1SD,  $n = 9$ ) of sample Hg mass. We combusted NIST SRM 1515 (Apple Leaves,  $44 \pm 4$  ng/g) with recoveries ranging from 95.1% to 96.2% ( $n = 2$ ) and NIST SRM 1575a (Pine Needles,  $39.9 \pm 7$  ng/g) with recovery of 108.6% ( $n = 1$ ), all well within certified values. Combustion solutions were further concentrated using large-scale purge and trap procedures in order to combine Hg from multiple combustion preparations, to further remove matrix interferences, and to achieve the 1- to 5- $\mu$ g/g concentrations ideal for isotopic analysis at the University of Michigan (Demers et al., 2018). Purge and trap recovery of Hg from combustion solutions was 97.4% ( $\pm 1.2\%$ , 1SD,  $n = 12$ ). We also monitored the performance of the purge and trap system with procedural blanks and procedural standards that were prepared in the same manner as samples. The purge and trap procedural blank contained 0.02 ng of Hg, corresponding to <0.2% of Hg in final sample solutions, on average. Purge and trap procedural standard recoveries were 94.2% and 103% for the 12 and 20 ng Hg standards, respectively.

Mercury isotope ratios were measured using a multiple collector inductively coupled plasma mass spectrometer (Nu Plasma I, Nu Instruments) using continuous flow cold-vapor generation via inline  $\text{SnCl}_2$  reduction (Blum & Bergquist, 2007; Lauretta et al., 2001); additional details can be found in supporting information (Text S1). We report isotopic compositions as per mil (‰) deviations from the average of NIST SRM 3133 bracketing standards using delta notation:

$$\delta^{\text{xxx}}\text{Hg} (\text{\textperthousand}) = \left\{ \left[ \left( \frac{\text{xxxHg}}{\text{Hg}^{198}} \right)_{\text{unknown}} / \left( \frac{\text{xxxHg}}{\text{Hg}^{198}} \right)_{\text{NIST SRM 3133}} \right] - 1 \right\} * 1,000 \quad (1)$$

where xxx is the mass of each Hg isotope between  $^{199}\text{Hg}$  and  $^{204}\text{Hg}$ . We use  $\delta^{202}\text{Hg}$  to report mass-dependent fractionation (MDF). Mass-independent fractionation (MIF) is reported as the deviation of the isotope ratio from the theoretically predicted values based on the kinetic MDF law and measured  $\delta^{202}\text{Hg}$  values (Blum & Bergquist, 2007). MIF is reported in “capital delta” notation ( $\Delta^{\text{xxx}}\text{Hg}$ ) and is well approximated for small ranges in delta values ( $\leq 10\text{\textperthousand}$ ) by equation (2):

$$\Delta^{\text{xxx}}\text{Hg} (\text{\textperthousand}) \approx \delta^{\text{xxx}}\text{Hg} - (\delta^{202}\text{Hg} \times \beta) \quad (2)$$

where xxx is the mass of each Hg isotope ( $^{199}\text{Hg}$ ,  $^{200}\text{Hg}$ ,  $^{201}\text{Hg}$ , and  $^{204}\text{Hg}$ ) and  $\beta$  is a constant (0.252, 0.502, 0.752, and 1.493, respectively) (Blum & Bergquist, 2007). We characterized the uncertainty of Hg isotope measurements using a secondary standard (UM-Almaden, equivalent to NIST RM 8610), as well as with procedural standards using reference materials (i.e., apple leaves and pine needles) (Text S1 and Table S1). Overall, the measured isotopic composition of Hg in reference materials compared well with the University of Michigan long-term averages (Blum & Johnson, 2017) (Text S1 and Table S1).

#### 2.4. Statistical Analysis

To determine if there were latitudinal differences in tree ring Hg mass and concentration, we employed multiple one-way analysis of variance across the three regions (North, Central, and South) using Tukey's honest significant difference criterion in Matlab (Mathworks, Natick, MA). Tree species may accumulate Hg at different rates, so we applied this test only on a species-specific basis. This limits the sample size, and since Tukey's honest significant difference criterion is known to be conservative when sample sizes differ (which may be the case when rings for certain decades are present in some trees and not others), we used  $p < 0.10$  as the threshold to establish significance. Linear regressions to determine the strength and significance of the relationship between tree growth rate and Hg concentration as well as Hg mass for each species were also determined with Matlab, and we used  $p < 0.05$  as the threshold to establish this significance. To assess the slope of the relationship between  $\Delta^{199}\text{Hg}$  and  $\Delta^{201}\text{Hg}$  values, we utilized a widely used maximum likelihood regression technique (York et al., 2004) that accounts for analytical uncertainty associated with both X and Y variables.

### 3. Results

#### 3.1. Tree Ages and Growth Rates

Ages of the sampled trees varied by species. Pitch pines were generally the youngest, with earliest rings typically between 1910 and 1930, shortly before the establishment of the Park. The oldest northern red oaks dated as far back as the 1830s, while the oldest white oaks dated to 1803 and 1812 (Table S2). Mean growth rates, determined for each of the 10-year Hg analysis periods for each species (Figure S1), ranged from 0.56 to 2.82 cm per 10-year increment. Prior to 1900, growth rates for the two species that were present (northern red oak and white oak) were the lowest for the period of record, with means typically less than 1.0 cm per decade. A clear increase in growth rates began for all species in the 1924–1933 period, with maximum rates (mean above 2.0 cm per decade for all species) measured in the 1945–1953 period. The increase in growth was likely caused by the release from competition/shading, which occurred after the demise of the American Chestnut, *Castanea dentata*, (Berish & Ragsdale, 1985), which occurred in the 1920–1930 time frame within the region encompassing Shenandoah National Park (Gravatt, 1949). A return to moderate growth rates (means range between 1 and 2 cm per decade) was evident by the late 1960s and was maintained thereafter for all species, in all regions.

#### 3.2. Tree Ring Concentrations and Burdens

Elemental accumulation in tree rings is traditionally expressed in terms of mass fraction or the more commonly used term, concentration (e.g., ng element per gram dry weight of core). Elemental burdens, calculated by multiplying element concentrations by core mass per time increment (e.g., ng element per temporal increment), have also been presented for trace metals (Baes & McLaughlin, 1984) and sulfur (Frelich et al., 1989) as it is possible for concentration decreases to result from constant elemental accumulation in larger annual rings (Berish & Ragsdale, 1985). Since it is somewhat ambiguous about which metric may be most appropriate for documenting Hg accumulation, both Hg concentrations as well as burdens (i.e., masses) are presented and evaluated.

Across all species, the average Hg concentration was 0.876 ng/g. Tree ring concentrations in individual cores ranged from −0.539 to 4.427 ng/g (negative concentrations, although physically unrealistic, can result from digestion blank subtraction). Pitch pine was found to have the highest overall concentrations (average of 1.305 ng/g, with a range from −0.539 to 4.427 ng/g), followed by N. red oak (average of 1.035 ng/g, with a range from 0.242 to 4.007 ng/g; not statistically different than pitch pine), and then white oak (average of 0.461 ng/g, with a range from −0.263 to 1.862 ng/g). Hg concentrations were not significantly related to core mass for pitch pine and N. red oak ( $p = 0.08$  and  $0.16$ , respectively, Figures S2a and S2c). However, Hg concentrations were negatively related to core mass for white oak (i.e., greater growth was associated with lower concentrations;  $p = 0.02$ , Figure S2e).

In terms of Hg mass, the average 10-year increment had a value of 0.195 ng across species, with a range from −0.054 to 2.656 ng. Similar to the rank order of Hg concentrations, pitch pine was found to have the highest Hg mass accumulation per 10-year increment (average of 0.304 ng, with a range from −0.054 to 2.656 ng). N. red oak was the next highest (average of 0.227 ng, with a range from 0.029 to 1.271 ng), followed by white oak (average of 0.096 ng, with a range from −0.013 to 0.362 ng). Hg mass had a positive significant relationship with core mass for all species ( $p < 0.0001$  for both pitch pine and N. red oak, and  $p < 0.01$  for white oak, Figures S2b, S2d, and S2f).

Temporal variability in tree ring Hg concentrations exhibited some differences between species (Figures 2(a), 2(c), and 2(e)). The highest concentrations of Hg in pitch pine were found in the earliest portions of their record, from the 1930s to the 1950s (Figure 2(a)). This was also a time of relatively high concentrations in N. red oak, although this was a secondary peak relative to the highest concentrations found in the most recent decade (Figure 2(c)). White oak exhibited high variability in Hg concentrations during the 1890s to 1920s, but overall, the trends were relatively subdued (Figure 2(e)). Meanwhile, temporal variability of Hg mass (Figures 2(b), 2(d), and 2(f)) exhibited a primary peak for all species occurring during the 1924–1953 time frame, with a secondary peak for both oak species over the last several decades. An alternative plot for Figure 2, showing time series information for individual trees, is provided in the supporting information (Figure S3).

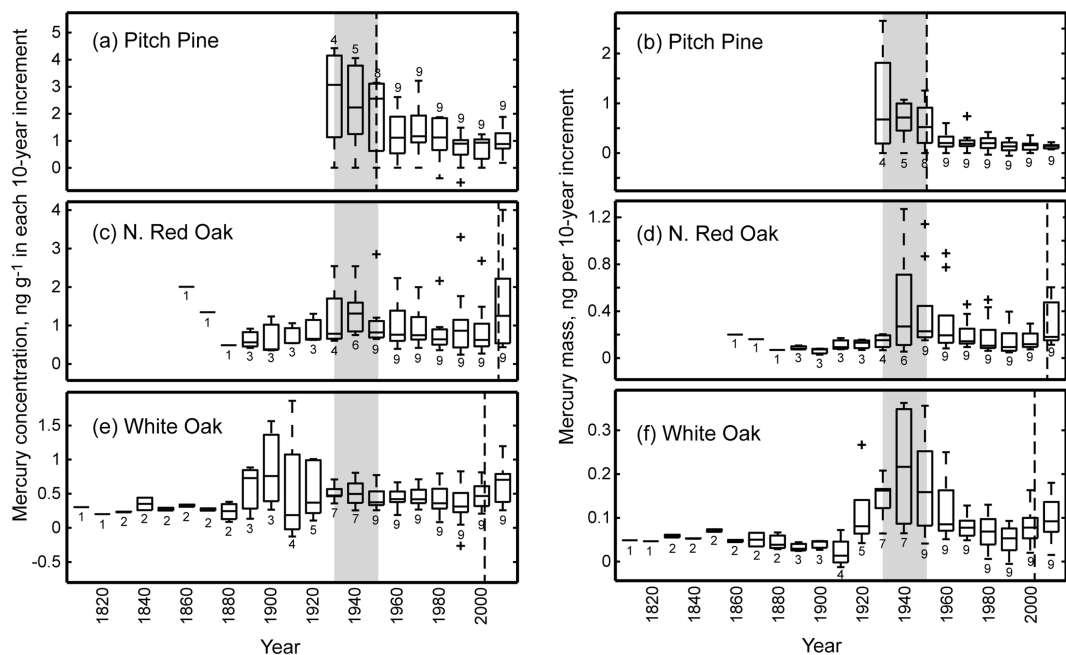


**Figure 2.** Box plot of tree ring mercury concentrations (ng/g), left column, and mercury mass (ng), right column, in decadal increments for (a, b) pitch pine, (c, d) northern red oak, and (e, f) white oak. Sample sizes are noted above or below each bar (maximum: 3 sites  $\times$  3 individuals/site = 9 core increments). Horizontal lines represent the median values, boxes bound the 25th to 75th percentiles, whiskers extend to 1.5 times the interquartile range, and the “+” symbol represent outliers. Dashed vertical lines denote sapwood-heartwood boundary, identified by color change. The gray shaded area represents period of active hg use at the DuPont plant in Waynesboro, Virginia.

### 3.3. Mercury Isotopic Composition of Bole Wood

The Hg isotopic composition of bole wood samples is reported in full in Table S3 and is summarized in Figures 3 and S5 and S6. Overall, tree ring Hg was characterized by negative  $\delta^{202}\text{Hg}$  values that varied by tree species. Northern red oak bole wood  $\delta^{202}\text{Hg}$  values clustered tightly ( $-1.81\text{\textperthousand}$  to  $1.84\text{\textperthousand} \pm 0.06\text{\textperthousand}$ , 2SD), while white oak  $\delta^{202}\text{Hg}$  values varied more widely ( $-1.66\text{\textperthousand}$  to  $-1.95\text{\textperthousand} \pm 0.06\text{\textperthousand}$ , 2SD), and pitch pine  $\delta^{202}\text{Hg}$  values were significantly lower ( $-2.14$  to  $-3.61\text{\textperthousand} \pm 0.06\text{\textperthousand}$ , 2SD). While there was no temporal trend in the isotopic composition of red oak tree ring Hg, both white oak and pitch pine bole wood shifted to relatively high  $\delta^{202}\text{Hg}$  values from the pre-1929 time frame through the modern era (Figure S5). This shift toward isotopically lighter Hg in older tree ring samples coincided with higher bole wood Hg concentrations (slope =  $-0.86 \pm 0.12$  (1SE),  $r^2 = 0.88$ ,  $p < 0.001$ ,  $n = 9$ ). Most bole wood samples also displayed significant negative  $\Delta^{199}\text{Hg}$  values ranging from  $-0.14\text{\textperthousand}$  to  $-0.39\text{\textperthousand}$  ( $\pm 0.05\text{\textperthousand}$ , 2SD), similar to atmospheric gaseous mercury, except for pitch pine from the modern era, which had a  $\Delta^{199}\text{Hg}$  value of  $+0.25\text{\textperthousand} \pm 0.05\text{\textperthousand}$  (2SD), more similar to typical values for precipitation (Table S3) (e.g., Demers et al., 2013; Demers et al., 2015; Enrico et al., 2016; Fu et al., 2016; Gratz et al., 2010). A linear regression of  $\Delta^{199}\text{Hg}$  versus  $\Delta^{201}\text{Hg}$  for all bole wood samples yielded a slope of  $1.05 \pm 0.05$  (1SE), with the y intercept offset from the origin ( $-0.15\text{\textperthousand} \pm 0.01\text{\textperthousand}$ , 1SE), consistent with photochemical reduction processes (Blum et al., 2014) (Figure S6).

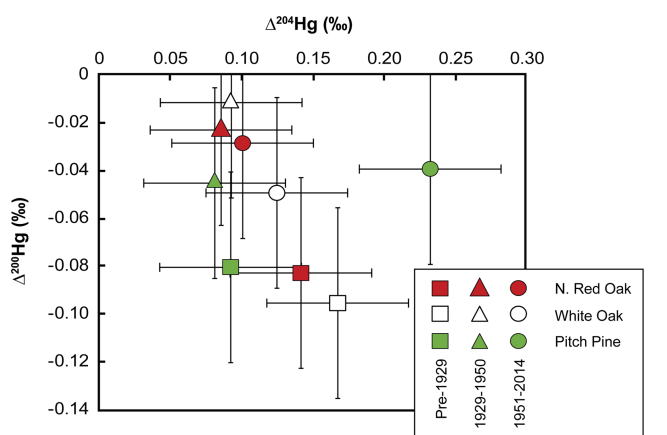


**Figure 3.** Even-mass number mass-independent fractionation (even-mass MIF) in tree ring hg composites across all regions of Shenandoah National Park. Symbols indicate time periods (pre-1929, 1929–1950, and 1951–2014), and colors represent tree species (northern red oak, white oak, and pitch pine). Analytical uncertainty (2 $\sigma$ ) for individual data points is based on analytical performance of within-run UM-Almaden and procedural standards and is represented by the black cross hairs (see section 2 and text S1 for details).

All bole wood samples had negative  $\Delta^{200}\text{Hg}$  values and positive  $\Delta^{204}\text{Hg}$  values, most of which were significantly different from zero (Figure 5), similar to even-mass number MIF (hereafter, even-mass MIF) observed in atmospheric gaseous Hg (e.g., Demers et al., 2013; Enrico et al., 2016;

Gratz et al., 2010). On average, even-mass MIF signatures were shifted closer to zero in tree rings from the 1929–1950 period coinciding with local industrial activity at the DuPont plant, relative to tree rings from before 1929 and during the modern era (1951–2014) (Figure 3).

## 4. Discussion

### 4.1. Tree Ring Hg Concentrations and Burdens

Tree ring Hg concentrations measured in Shenandoah National Park (from below detection to 4.4 ng/g) are within the range of previously reported Hg concentrations in tree woody tissue, based on the literature review of Wright et al. (2014) and subsequent studies. Concentrations are very similar to the mean concentrations measured in pine species in California and Nevada (0.4 to 5.8 ng/g) by Wright et al. (2014) and Peckham et al. (2019) and white spruce in northwestern Canada (0.3 to 3.2 ng/g) by Clackett et al. (2018). They were also similar to bulk bole wood concentrations in hardwood and conifer species in the northeastern United States (0.4 to 2.8 ng/g) reported by Yang et al. (2018). Studies conducted in the immediate vicinity of known industrial Hg sources have reported higher tree ring Hg concentrations than those measured in SHEN. For example, Navratil et al. (2018) found elevated peaks in tree ring Hg concentrations near a gold mine (14 ng/g), a chlor-alkali plant (13 ng/g), and a smelter (38 ng/g) in the Czech Republic. Even higher concentrations have been reported, such as the 13- to 644-ng/g range reported for trees near water bodies downstream of petrochemical plants and paper mills in southeastern Louisiana (Becnel et al., 2004).

In SHEN, higher Hg concentrations were found in pitch pine compared with *N. red* oak and white oak. This is consistent with the findings of Obrist et al. (2012), who measured woody tissue Hg concentrations and reported higher values in a coniferous forest compared with an adjacent deciduous forest that experienced approximately the same Hg deposition. Possible reasons for these differences (e.g., tree morphology, leaf physiology, or foliar phenology) remain speculative. It should be noted, however, that it is not always the case that Hg concentrations in conifers are higher than in deciduous species, as Yang et al. (2018) found that bole wood Hg concentrations in yellow birch tended to equal or exceed the concentrations in nearby spruce, pine, and fir trees.

The lack of a significant relationship between Hg concentration and core mass for pitch pine and *N. red* oak indicates that greater radial growth does not dilute Hg (or less growth does not concentrate Hg), which might imply that Hg concentration is an appropriate metric to evaluate trends for those species. In contrast, Hg concentration in white oaks had a significant, negative relationship with tree core mass, which indicates that greater radial growth may have diluted Hg in that species (although the variability explained was small;  $r^2 = 0.04$ , Figure S2e). As a note of caution, such inferences would hold only if the ambient atmospheric mercury concentrations were stationary throughout the period of analysis. And since it is our goal to leverage the archived tree ring Hg to estimate how Hg exposure has changed over time, this introduces some logical circularity in using correlation analysis to evaluate the potential for biodilution or bioconcentration.

Another issue that could compound the difficulty in interpreting these correlations is one of multicollinearity (e.g., the timing of peak growth may happen to correspond with the timing of peak Hg exposure). The significant positive relationship between Hg mass and tree growth for all tree species suggests that Hg mass, as a metric, may be biased by degree of tree growth. Indeed, since foliar uptake is the dominant pathway for Hg accumulation in tree wood (Arnold et al., 2018), photosynthetic processes regulating tree productivity are inherently intertwined with the processes regulating Hg uptake and translocation. This does not necessarily mean, however, that the amount of Hg accumulation in tree rings scales linearly with growth. If biodilution were to occur, then Hg mass could be a better metric for documenting historical Hg exposure. For this reason, we consider both metrics and place emphasis on the tree species for which both Hg concentration and Hg mass have similar temporal trends.

Tree species were selected for sampling based on their common ridgeline presence over the entirety of SHEN. The uniqueness of their physiologies should be noted with respect to the potential for tree ring Hg accumulation. For example, the degree of tylosis, which occurs during the sapwood-heartwood transformation, is greater in white oak than in red oak. This process, which is associated with lower water content in wood vessels, has been cited as a reason that white oak may be a more reliable option for dendrochemistry studies (Cutter & Guyette, 1993). Also, the number of rings in sapwood is much greater in pitch pine compared

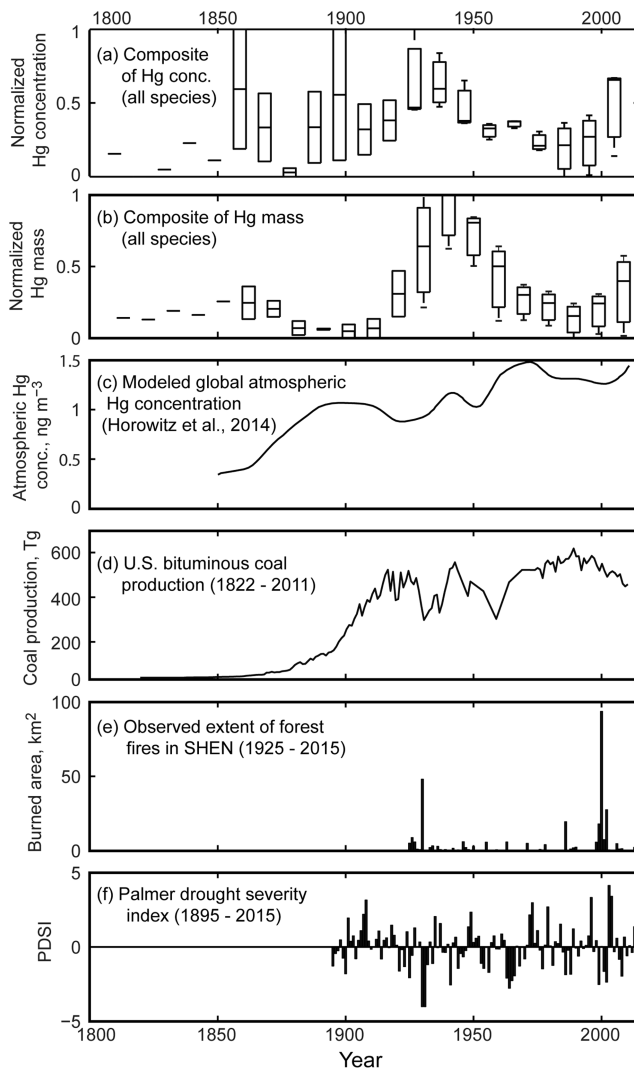


**Figure 4.** Temporal variability in a normalized composite mean hg concentration by decadal interval for the three tree species, b normalized composite mean hg mass by decadal interval for the three tree species, c modeled global atmospheric hg concentration after Horowitz et al. (2014), d bituminous coal production in the United States (1921–1945 data, United States Bureau of the Census, 1949; 1945–2011 data, U.S. Department of Energy, 2011), e area burned by forest fires in SHEN (1930–1989 data, Shenandoah National Park Resource Management Records, catalog number SHEN 47033, fire atlas 1930–1989; 1990 to present data, D. Hurlbert NPS, personal communication, 2016), and f annual palmer drought severity index (PDSI) for Virginia, region 3 (NOAA, 2016).

with the hardwood species (Figure 2). Since radial permeability is enhanced in sapwood, this may contribute to reduced temporal precision in the elemental concentrations measured in this region (Cutter & Guyette, 1993). The highest Hg concentrations in pitch pine were found on the heartwood side of the heartwood-sapwood boundary (Figures 2 (a) and 2(b)), but it is unclear to what extent, if any, this boundary might have had on these measured concentrations. In another study conducted using *Pinus* species, Wright et al. (2014) found higher Hg concentrations in the sapwood relative to the heartwood, so there does not appear to be directional consistency in any radial translocation across this boundary. Factors associated with the disparate tree physiologies should be taken into consideration when interpreting time series on a species-specific basis (Figure 2) or in aggregate form (Figures 4(a) and 4(b)).

#### 4.2. Temporal Trends in Tree Ring hg Accumulation

A limited number of prior studies have used dendrochemistry to estimate historical levels of ambient atmospheric Hg. For studies that were conducted in the absence of known local sources, trends in tree ring Hg have generally shown gradual increases since the time of the Industrial Revolution (Clackett et al., 2018; Peckham et al., 2019; Wright et al., 2014). Such behavior might be expected in Shenandoah National Park, but similar trends were not observed (Figure 2). This is somewhat surprising, given that modern rates of Hg deposition ( $Hg^0 + Hg^{2+}$ ) in the southeastern United States are approximately 3 times higher than in western North America (Corbitt et al., 2011), where the other studies were conducted. On the other hand, no other measured environmental parameters in SHEN (atmospheric, biological, terrestrial, or aqueous) have been found to have particularly elevated Hg concentrations relative to other U.S. locations. Most notable from the observed time series (Figure 2), with some degree of consistency between species, is that trees exhibited peaks in Hg accumulation near the middle of the twentieth century.

The development of a composite curve allows for the identification of temporal trends across species. Since species accumulate Hg at different rates, we normalize the values for each species by their minimum and maximum decadal values such that they span the range [0 to 1]. The composite curve for Hg concentration (Figure 4(a)) includes several decades with large variance between species in the early portion of the time series. The highest mean values were found in the 1934–1943 and 2004–2013 decadal increments. The composite curve for Hg mass in decadal increments indicates subtly increasing tree ring Hg accumulation beginning just after the turn of the century, with a clear peak during the 1930s through 1950s (Figure 4(b)). This raises questions about what regional- to global-scale drivers could potentially contribute to these observed trends.

Estimates of global atmospheric Hg concentrations have been made by Horowitz et al. (2014) based on worldwide emission inventories coupled with a global biogeochemical model (Figure 4(c)). Although there is a small peak in atmospheric Hg concentrations during the 1940s, which Horowitz et al. (2014) attribute to chemical production for munitions during World War II, global atmospheric Hg concentrations at this time were lower than the peak reached over more recent decades. Composite Hg trends do indicate higher Hg accumulation in SHEN trees over recent decades, but a much larger peak is apparent during the 1930s through 1950s. A regional-scale candidate for the observed behavior is the burning of fossil fuels from within the SHEN airshed, which extends into the industrial midwestern region of the United States. However, the pattern of Hg accumulation in SHEN trees does not appear to be consistent with U.S. bituminous coal

production alone (Figure 4(d)), which has a trend similar to that of global atmospheric Hg concentrations. One difference is that U.S. bituminous coal production has decreased since 1990 (U.S. EIA, 2012), whereas global atmospheric Hg concentrations have continued to rise, reflecting increased Hg emissions from developing countries. The inconsistency between the SHEN tree ring Hg time series and global/regional trends suggests that other, perhaps, local factors may have contributed to the observed peak during the 1930s to 1950s.

Forest fires are known to volatilize and redeposit Hg on a local to regional basis (Burke et al., 2010; Engle et al., 2006; Friedli et al., 2003; Witt et al., 2009). Data from SHEN reveal large areas burned by wildfire in 1930 (Figure 4(e)), which followed a multiyear drought, as measured by the Palmer Drought Severity Index (Figure 4(f)). The impact from wildfire is not identifiable, however, since even more expansive wildfires in the late 1990s did not result in similar, concomitant increases in tree core Hg accumulation. Climate variability itself could be a potential factor in influencing both the Hg mass and Hg concentration in tree rings. However, climate is also not a leading candidate, since the tree ring Hg peak is not associated with any obvious decadal-scale climate anomalies (Figure 4(f)).

#### 4.3. A Potential Local Source

A known source of Hg pollution in the region is related to the use of mercuric sulfate in the production of Rayon between 1929 and 1950 at the E. I. DuPont de Nemours (DuPont) plant in Waynesboro, VA, located at the southern end of SHEN (Figure 1). Elemental and ionic Hg were released directly into the South River and into the floodplain soils near the plant. In 1984, DuPont agreed to fund a 100-year monitoring program, which has since supported research (e.g., over 100 peer reviewed publications available at <http://soutriverscienceteam.org/resources/journal-articles/>) and the development of remedial strategies for on-site and down-river Hg contamination. Whether or not the Hg used at this industrial site could have escaped to the atmosphere has never been fully investigated. According to a representative from DuPont (M. Liberati, personal communication, 16 February 2016), a closed retort furnace that was used in the catalysis process captured and recycled about 99% of the Hg, while the remaining organic-bound Hg was disposed in the form of sludge. Indeed, there is incentive to minimize fugitive Hg emissions, since almost all of the collected Hg could be reused. However, the technology used at the time may have been inadequate in preventing such losses. Of note, a 1942 patent for a retort furnace specifically referred to an improved design to capture Hg gas, “whereby the escape of unhealthful, noxious vapors from the apparatus will be eliminated” (U.S. Patent #2273929 A).

The alignment of the SHEN tree ring Hg peak with the timing of Hg use at the Waynesboro DuPont plant (gray shaded areas in Figure 2) may be coincidental or it may point to a previously undocumented local source. As suggested by Peckham et al. (2019), spatial trends in tree ring Hg concentrations can be used to detect spatial trends in atmospheric Hg availability.

Focusing on the time frame where there appears to be a primary peak in Hg accumulation (1924–1953), we look for latitudinal trends of tree ring Hg within SHEN (Figure 5). During this period, Hg concentrations in pitch pine (Figure 5(a)) and *N. red* oak (Figure 5(c)) increased in a north-to-south direction (i.e., they were found to be higher in the southern portion of the Park, in the vicinity of Waynesboro). For both species, Hg concentrations were significantly higher in the southern region compared with the northern region of the Park ( $p < 0.1$ ). This latitudinal gradient was not as obvious for white oak, which had the lowest Hg concentrations (Figure 5(e)). The southern site was found to be significantly higher than the central site, but it was not significantly different from the northern site. In terms of Hg mass, *N. red* oak had significantly higher levels in the southern region of the Park (Figure 5(d)), but no significant differences were found for pitch pine (Figure 5(b)) and white oak (Figure 5(f)) along the latitudinal gradient. Overall, however, the latitudinal analysis does provide some evidence of Hg enrichment in the southern region of SHEN, which diminishes to the north.

While it is reasonable to expect that smokestack emissions in Waynesboro could enhance deposition in the nearby mountains, it is less clear if emissions could potentially impact the sites further to the north. An analysis of contemporary (2008–2011) wind data from an airport near Waynesboro shows that the dominant wind direction is parallel with the orientation of the Blue Ridge Mountains (Figure S4). Results from the Hybrid Single-Particle Lagrangian Integrated Trajectory (HYSPLIT) model (Draxler & Hess, Sept., 2014)

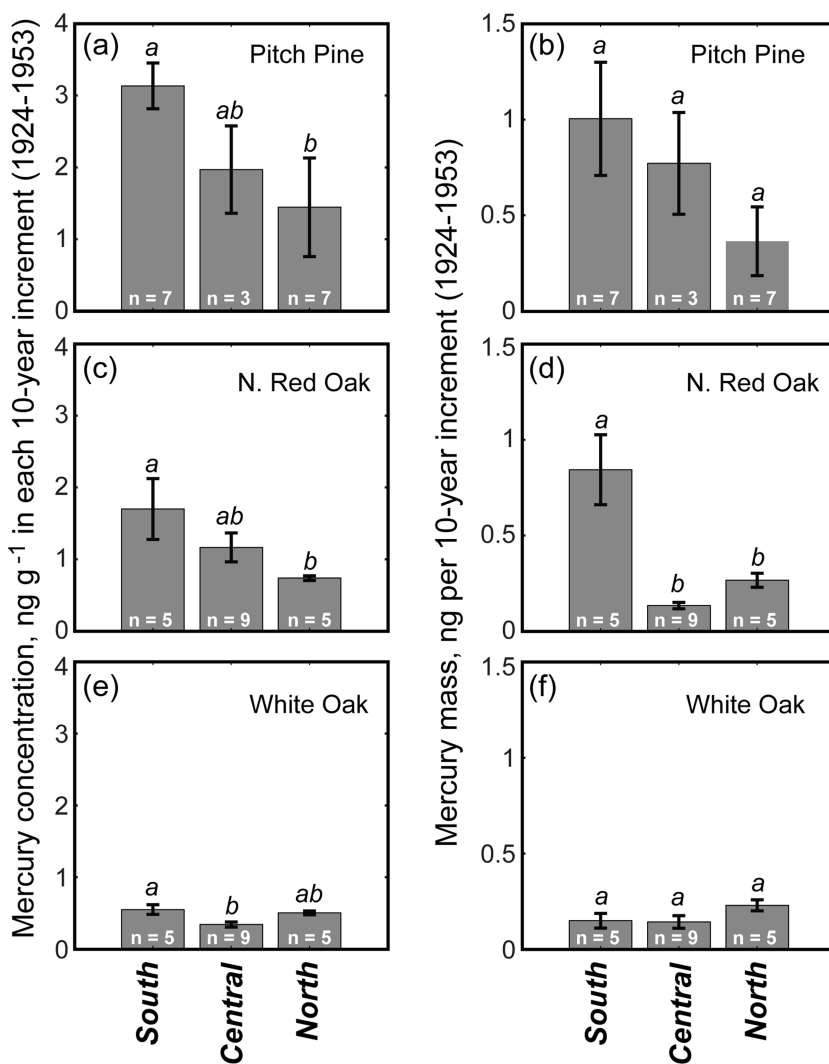


**Figure 5.** Latitudinal trends in (a, c, and e) mercury concentration and (b, d, and f) mercury mass for 10-year tree core increments during the 1924–1953 time frame, covering the period of active hg use at the DuPont plant in Waynesboro. Bar plots show means and standard errors. Sample sizes are noted within each bar (maximum: 3 individuals  $\times$  3 decadal core increments/individual = 9 core increments).

(see Text S2 for more details) for randomly selected days when the wind was coming from this dominant direction indicate that neutrally buoyant emissions from Waynesboro could potentially impact the central and northern sites, albeit to a lesser extent than the southern site (Figure S4). This is consistent with the latitudinal gradient of Hg observed in tree rings.

#### 4.4. Mercury Isotopes in Tree Rings

##### 4.4.1. Tree Rings as Temporal Records of Atmospheric hg Isotopic Composition

Mercury isotopes can be used to differentiate between sources of atmospheric Hg. Relative MDF signatures ( $\delta^{202}\text{Hg}$  values) are useful for evaluating the influence of background versus anthropogenic atmospheric Hg sources. Background atmospheric gaseous Hg is characterized by relatively heavy Hg isotope signatures (high  $\delta^{202}\text{Hg}$  values), whereas anthropogenic influences typically drive  $\delta^{202}\text{Hg}$  to relatively low values (Demers et al., 2015; Fu et al., 2014; Fu et al., 2016; Gratz et al., 2010; Yu et al., 2016). Odd-mass MIF is particularly useful for differentiating between precipitation sources characterized by positive  $\Delta^{199}\text{Hg}$  (and  $\Delta^{201}\text{Hg}$ ) values and atmospheric gaseous Hg sources characterized by negative  $\Delta^{199}\text{Hg}$  (and  $\Delta^{201}\text{Hg}$ ), predominantly resulting from photochemical processes, as reviewed by Blum et al. (2014). Even-mass MIF ( $\Delta^{200}\text{Hg}$  and  $\Delta^{204}\text{Hg}$ ) also can be used to distinguish between precipitation and atmospheric gaseous Hg

sources, with atmospheric gaseous Hg having small negative  $\Delta^{200}\text{Hg}$  and positive  $\Delta^{204}\text{Hg}$  values, opposite in sign but complementary to precipitation signatures (Demers et al., 2013; Gratz et al., 2010). Additionally, even-mass MIF signatures can be utilized to identify emissions stemming from industrial use of elemental Hg(0), which would typically have little to no even-MIF signature (Sun et al., 2016), as even-mass MIF anomalies are thought to be produced exclusively in the upper atmosphere during oxidation reactions followed by scavenging of oxidized species onto droplets or particles (Chen et al., 2012; Sun et al., 2016). Thus, even-mass MIF acts as a more conservative tracer of atmospheric Hg as it moves into the terrestrial environment, whereas nearly all kinetic reactions involving Hg result in MDF with the products being isotopically lighter (lower  $\delta^{202}\text{Hg}$  values) and the residual reactant pool becoming isotopically heavier (higher  $\delta^{202}\text{Hg}$  values) (Blum et al., 2014). Notably, atmospheric gaseous Hg isotopes undergo strong MDF during foliar uptake, resulting in  $-2.3\text{\textperthousand}$  to  $-2.9\text{\textperthousand}$  shifts in  $\delta^{202}\text{Hg}$  values (Demers et al., 2013; Enrico et al., 2016).

The isotopic composition of Hg in tree rings from the modern era (1951–2014) in both deciduous and coniferous species in this study is broadly similar to the Hg isotopic composition typically observed in North American foliage (Demers et al., 2013; Olson et al., 2019; Woerndle et al., 2018; Zheng et al., 2016) (Figure S5 and Tables S3 and S4). This is consistent with bole wood Hg being derived predominantly from atmospheric gaseous Hg that accumulates in foliage and is subsequently translocated downward via the phloem (e.g., Arnold et al., 2018). However, our analyses also revealed colocated species-specific differences in bole wood  $\delta^{202}\text{Hg}$  values (Table S3 and Figure S5), similar to the widely varying  $\delta^{202}\text{Hg}$  values in foliage across the world (Table S4). Broadleaf deciduous species have been shown to have  $\delta^{202}\text{Hg}$  values that range from  $-1.12 \pm 0.06\text{\textperthousand}$  to  $-2.05 \pm 0.35\text{\textperthousand}$  (1SD), whereas there is some evidence that Hg accumulated in coniferous species tends to be isotopically lighter, with  $\delta^{202}\text{Hg}$  values ranging from  $-1.53\text{\textperthousand} \pm 0.06\text{\textperthousand}$  to  $-2.72 \pm 0.25\text{\textperthousand}$  (1SD) (Demers et al., 2013; Enrico et al., 2016; Liu et al., 2019; Olson et al., 2019; Woerndle et al., 2018; Zheng et al., 2016). This is consistent with the lower  $\delta^{202}\text{Hg}$  values observed in coniferous pitch pine bole wood relative to the broadleaf deciduous oaks in this study (Figure S5 and Table S3). Thus, it is plausible that there are species-specific differences in MDF of atmospheric Hg during foliar uptake, possibly due to differences in the organic ligands that bind Hg within the stomatal cavity, as ligand chemistry has been shown to affect fractionation during other processes (e.g., Zheng & Hintelmann, 2010). Taken together, species-specific differences in isotopic fractionation during foliar uptake may account for some of the differences in colocated species-specific bole wood Hg isotopic composition in this study.

Species-specific differences in bole wood Hg isotopic composition could also result from differences in atmospheric Hg sources to which individual tree species are exposed. Atmospheric total gaseous Hg (TGM) signatures can vary by as much as 1%, or more, at individual locations over daily, monthly, or seasonal timescales as TGM sources change with prevailing meteorological conditions (e.g., Demers et al., 2013; Fu et al., 2016; Gratz et al., 2010; Yu et al., 2016). Anthropogenic sources drive the composition of atmospheric TGM toward lighter  $\delta^{202}\text{Hg}$  values (Demers et al., 2015; Fu et al., 2016; Gratz et al., 2010; Yu et al., 2016), which would be translated into relatively light  $\delta^{202}\text{Hg}$  during fractionation during foliar uptake (Demers et al., 2013; Enrico et al., 2016). Although colocated tree species would be exposed to similar sources of TGM at any given time, their effective exposures could differ due to differences in stomatal conductance and seasonality of photosynthesis or their propensity for nonstomatal (cuticular) uptake, as observed in *Populus tremuloides* (Arnold et al., 2018; Stamenkovic & Gustin, 2009). For example, temperate coniferous evergreen species generally have lower photosynthetic rates but can be photosynthetically active throughout the year (e.g., Nippert et al., 2004). Thus, evergreen species likely incorporate TGM during the fall, winter, and early spring when deciduous species are leafless, and this year-round exposure could further influence foliar and bole wood Hg isotopic composition. Specifically, in temperate regions, heating demands during winter increase Hg(0) emissions related to coal combustion (Jiskra et al., 2018; Temme et al., 2007; Weigelt et al., 2015), which would drive atmospheric Hg(0) to lower  $\delta^{202}\text{Hg}$  values (e.g., Sun, 2019). Late season and winter uptake of atmospheric Hg by evergreen species would likely accumulate isotopically lighter Hg than foliar uptake during the peak growing season, on average. Thus, differences in seasonal exposure could further lead to lower  $\delta^{202}\text{Hg}$  values reported in the literature for coniferous foliage and observed during this study in pitch pine bole wood.

Tree anatomy and physiology may also influence the MDF signatures of Hg isotopes in tree rings. The mechanisms underlying Hg translocation downward through the phloem, phloem-to-xylem lateral

transport, and subsequent potential radial translocation through sapwood rings and/or heartwood may also differ by tree species (e.g., Cutter & Guyette, 1993) and has not been studied. Whether these processes induce any MDF of Hg isotopes (subsequent to foliar uptake) likely depends on whether translocation processes involving Hg are accomplished by physical mass transfer, diffusion, or if Hg-associated sulfur-bearing compounds are chemically altered during transport and thus provide opportunities for fractionation during exchange of Hg among binding sites.

Despite the potential complexities of MDF associated with foliar uptake, resorption, and translocation,  $\delta^{202}\text{Hg}$  values in tree rings have the potential to track relative changes in the isotopic composition of atmospheric gaseous Hg and to lend insight into spatial and temporal shifts in sources of Hg emissions to the atmosphere. Given the apparent species-specific differences in MDF during foliar uptake, as well as potential differences in fractionation during translocation, species-specific approaches using tree rings to quantify relative changes in atmospheric Hg isotopic composition are likely advisable. Moreover, deciduous tree species may better reflect growing season atmospheric Hg concentrations and isotopic composition, while evergreen species may better reflect mean annual averages.

#### 4.4.2. Mercury Isotopic Evidence of a Local Source

Mercury isotopes have previously been used to differentiate contributions of anthropogenic versus background sources of Hg in stream sediments (Donovan et al., 2014; Washburn et al., 2017, 2018), lake sediments (Cooke et al., 2013; Gray et al., 2015; Guédron et al., 2016; Kurz et al., 2019; Ma et al., 2013), and peat bogs (Enrico et al., 2016; Enrico et al., 2017). In this study, dendrochronological tree ring Hg isotopic composition provides evidence that SHEN trees have been impacted by regional anthropogenic and local industrial Hg emissions, particularly during the 1930s to 1950s in conjunction with activities at the DuPont plant. Notably, Hg released to downstream sediment and surface waters from the DuPont plant has been found to be isotopically distinct from regional background sources (Washburn et al., 2017, 2018). High-concentration sediment (3 to 65  $\mu\text{g/g}$ ) reflecting this industrial source of Hg was found to have  $\delta^{202}\text{Hg}$  values ( $-0.63 \pm 0.03\text{‰}$ , 1SD) (Washburn et al., 2017) similar to that of bulk mercury ores ( $-0.56 \pm 0.63\text{‰}$   $\delta^{202}\text{Hg}$ , 1SD) (Smith et al., 2008; Yin et al., 2013) and average commercial sources of liquid elemental Hg(0) ( $-0.38 \pm 0.34\text{‰}$   $\delta^{202}\text{Hg}$ , 1SD) (Sun, Streets, et al., 2016), with no discernable odd-mass or even-mass MIF. Mercury laden sludge produced during manufacturing at the DuPont plant was retorted on site to recover Hg for reuse (Carter, 1977; URS Corporation, 2015). Laboratory experiments have shown that the retorting process results in MDF only, releasing gaseous Hg(0) that is isotopically lighter than the initial feed stocks by as much as  $-0.8\text{‰}$   $\delta^{202}\text{Hg}$ , on average (Gray et al., 2013). This suggests that fugitive Hg(0) emissions from the DuPont retorting facility would have been in the vicinity of  $-1.4\text{‰}$   $\delta^{202}\text{Hg}$  with no MIF, prior to foliar uptake.

Tree ring Hg isotopic composition suggests that a local industrial source of atmospheric Hg contributed to peaks in tree ring Hg mass and concentration during the DuPont era (1929–1950). The exclusively positive  $\Delta^{204}\text{Hg}$  values in conjunction with the exclusively negative  $\Delta^{200}\text{Hg}$  values (Figure 3) reflect a predominance of tree ring Hg derived from atmospheric gaseous sources, consistent with foliar uptake. Mercury emitted to the atmosphere from local industrial sources, as described above for the DuPont plant, would have near-zero even-mass MIF values and would therefore plot near the origin in Figure 3. Meanwhile, Hg from the global atmospheric Hg reservoir would have longer atmospheric residence times and greater exposure to the upper atmosphere, which would result in more pronounced anomalies. We see that during the 1929–1950 time period, when Hg was being used at the DuPont plant, all tree species had even-mass MIF values that were closer to 0, suggesting that a greater portion of the Hg that accumulated in tree rings during this era was derived from a local industrial source.

## 5. Concluding Remarks

Previous studies that have quantified Hg in tree rings have either documented post-Industrial Revolution increases corresponding with gradually increasing Hg concentrations in the atmosphere (Clackett et al., 2018; Peckham et al., 2019; Wright et al., 2014) or peaks in tree ring Hg corresponding with the timing of local industrial sources (Hojdová et al., 2011; Maillard et al., 2016; Navratil et al., 2017; Navratil et al., 2018). The present study differs in that the main feature of the measured tree ring Hg time series derives

from a previously unidentified source. Thus, the application of Hg dendrochemistry described here depicts an unanticipated outcome and serves the purpose of hypothesis generation.

Temporal correspondence between the observed peaks in tree ring Hg accumulation and industrial Hg use at the DuPont plant in Waynesboro (Figure 2) provides some circumstantial evidence that they may be related. However, uneven responses in Hg accumulation with respect to tree species and coinciding enhanced growth rates associated with release from the chestnut blight (Figure S1) add some complexity to this assessment. Nevertheless, it is likely that any gaseous Hg released from Waynesboro would have been advected along SHEN (Figure S4), and latitudinal gradients in tree ring Hg (Figure 5) suggest that enhanced ambient Hg levels were present toward the southern end of the Park. Mercury isotopes provide complementary evidence that the Hg that accumulated in tree rings during the 1929–1950 time frame was significantly augmented by local industrial emissions (Figure 3). While this collective evidence may be compelling, additional information would be needed to more confidently attribute the observed SHEN tree ring Hg peak to Hg use at the DuPont plant (e.g., evaluation of Hg in pond sediment cores downwind from the plant). These findings do, however, raise questions about whether the contamination associated with this industrial site was limited to aqueous releases as previously assumed. Whereas research and remediation efforts have heretofore focused on acute Hg contamination within the flood plain and river, atmospheric transport may have dispersed Hg over a much larger geographical region.

This study represents the first attempt to use dendrochemistry to infer historical Hg exposure in an eastern U.S. forest. Considering that the eastern U.S. and in particular the Central Appalachians are subjected to high levels of Hg deposition relative to other parts of North America based on recent model results (e.g., Corbitt et al., 2011), information derived from tree rings can potentially provide important historical context for this region. Tree cores collected at other locations in the eastern United States might provide clearer signals of regional- to global-scale impacts if they are devoid of the local influences that were likely present in the current study. Also, the use of Hg isotopes for dendrochemical analysis is introduced here, which has the potential to develop into a powerful tool for differentiating local, regional, and global sources of atmospheric Hg that impact ecosystems over the historical record.

## Acknowledgments

This research was supported by a Grant (8104651) from the Appalachian Stewardship Foundation and the University of Virginia College Council Scholars Award. Data files and Matlab programs used in this analysis are archived at the University of Virginia's LibraData site (<https://doi.org/10.18130/V3/MBZ7SN>).

## References

Arnold, J., Gustin, M. S., & Weisberg, P. J. (2018). Evidence for nonstomatal uptake of hg by aspen and translocation of hg from foliage to tree rings in Austrian pine. *Environmental Science & Technology*, 52(3), 1174–1182. <https://doi.org/10.1021/acs.est.7b04468>

Baes, C. F., & McLaughlin, S. B. (1984). Trace-elements in tree rings: Evidence of recent and historical air-pollution. *Science*, 224(4648), 494–497. <https://doi.org/10.1126/science.224.4648.494>

Bank, M. S., Loftin, C. S., & Jung, R. E. (2005). Mercury bioaccumulation in northern two-lined salamanders from streams in the northeastern United States. *Ecotoxicology*, 14(1–2), 181–191. <https://doi.org/10.1007/s10646-004-6268-8>

Beal, S. A., Osterberg, E. C., Zdanowicz, C. M., & Fisher, D. A. (2015). Ice core perspective on mercury pollution during the past 600 years. *Environmental Science & Technology*, 49(13), 7641–7647. <https://doi.org/10.1021/acs.est.5b01033>

Becnel, J., Falgeust, C., Cavalier, T., Gauthreaux, K., Landry, F., Blanchard, M., et al. (2004). Correlation of mercury concentrations in tree core and lichen samples in southeastern Louisiana. *Microchemical Journal*, 78(2), 205–210. <https://doi.org/10.1016/j.microc.2004.06.002>

Berish, C. W., & Ragsdale, H. L. (1985). Chronological sequence of element concentrations in wood of *Carya* spp in the southern Appalachian mountains. *Canadian Journal of Forest Research-Revue Canadienne De Recherche Forestiere*, 15(3), 477–483. WOS: A1989T509600015. <https://doi.org/10.1139/x85-078>

Biester, H., Bindler, R., Martinez-Cortizas, A., & Engstrom, D. R. (2007). Modeling the past atmospheric deposition of mercury using natural archives. *Environmental Science & Technology*, 41(14), 4851–4860. <https://doi.org/10.1021/es0704232>

Blum, J. D., & Bergquist, B. A. (2007). Reporting of variations in the natural isotopic composition of mercury. *Analytical and Bioanalytical Chemistry*, 388(2), 353–359. <https://doi.org/10.1007/s00216-007-1236-9>

Blum, J. D., & Johnson, M. W. (2017). Recent developments in mercury stable isotope analysis. Non-traditional isotope geochemistry. *Reviews in Mineralogy and Geochemistry*, 82(1), 733–757.

Blum, J. D., Sherman, L. S., & Johnson, M. W. (2014). Mercury isotopes in earth and environmental sciences. *Annual Review of Earth and Planetary Sciences*, 42(1), 249–269.

Burke, M. P., Hogue, T. S., Ferreira, M., Mendez, C. B., Navarro, B., Lopez, S., & Jay, J. A. (2010). The effect of wildfire on soil mercury concentrations in Southern California watersheds. *Water, Air, and Soil Pollution*, 212(1–4), 369–385. <https://doi.org/10.1007/s11270-010-0351-y>

Butler, T., Likens, G., Cohen, M., & Vermeylen, F. (2007). Mercury in the environment and patterns of mercury deposition from the NADP/MDN mercury deposition network.

Carter, L. J. (1977). Chemical plants leave unexpected legacy for two Virginia rivers. *Science*, 198(4321), 1015–1020. <https://doi.org/10.1126/science.198.4321.1015>

Chellman, N., McConnell, J. R., Arriemo, M., Pederson, G. T., Aarons, S. M., & Csank, A. (2017). Reassessment of the upper Fremont glacier ice-core chronologies by synchronizing of ice-core-water isotopes to a nearby tree-ring chronology. *Environmental Science & Technology*, 51(8), 4230–4238. <https://doi.org/10.1021/acs.est.6b06574>

Chen, J. B., Hintemann, H., Feng, X. B., & Dimock, B. (2012). Unusual fractionation of both odd and even mercury isotopes in precipitation from Peterborough, ON, Canada. *Geochimica et Cosmochimica Acta*, 90, 33–46. <https://doi.org/10.1016/j.gca.2012.05.005>

Clackett, S. P., Porter, T. J., & Lehnher, I. (2018). 400-year record of atmospheric mercury from tree-rings in Northwestern Canada. *Environmental Science & Technology*, 52(17), 9625–9633. <https://doi.org/10.1021/acs.est.8b01824>

Colman, J. A., Waldron, M. C., Breault, R. F., & Lent, R. M. (1999). *Distribution and Transport of Total Mercury and Methylmercury in Mercury-Contaminated Sediments in Reservoirs and Wetlands of the Sudbury River*. Geological Survey: East-Central Massachusetts. U.S.

Converse, A. D., Riscassi, A. L., & Scanlon, T. M. (2010). Seasonal variability in gaseous mercury fluxes measured in a high-elevation meadow. *Atmospheric Environment*, 44(18), 2176–2185. <https://doi.org/10.1016/j.atmosenv.2010.03.024>

Converse, A. D., Riscassi, A. L., & Scanlon, T. M. (2014). Seasonal contribution of dewfall to mercury deposition determined using a micrometeorological technique and dew chemistry. *Journal of Geophysical Research: Atmospheres*, 119, 284–292. <https://doi.org/10.1002/2013jd020491>

Cooke, C. A., Hintelmann, H., Ague, J. J., Burger, R., Biester, H., Sachs, J. P., & Engstrom, D. R. (2013). Use and legacy of mercury in the Andes. *Environmental Science & Technology*, 47(9), 4181–4188. <https://doi.org/10.1021/es3048027>

Corbett, E. S., Jacob, D. J., Holmes, C. D., Streets, D. G., & Sunderland, E. M. (2011). Global source-receptor relationships for mercury deposition under present-day and 2050 emissions scenarios. *Environmental Science & Technology*, 45(24), 10,477–10,484. <https://doi.org/10.1021/es202496y>

Cutter, E. P., & Guyette, R. R. (1993). Anatomical, chemical, and ecological factors affecting tree species choice in dendrochemistry studies. *Journal of Environmental Quality*, 22, 611–619.

Daga, R., Guevara, S. R., Pavlin, M., Rizzo, A., Lojen, S., Vreča, P., et al. (2016). Historical records of mercury in southern latitudes over 1600 years: Lake Futalauquen, northern Patagonia. *Science of the Total Environment*, 553, 541–550. <https://doi.org/10.1016/j.scitotenv.2016.02.114>

Demers, J. D., Blum, J. D., Brooks, S. C., Donovan, P. M., Riscassi, A. L., Miller, C. L., et al. (2018). Hg isotopes reveal in-stream processing and legacy inputs in east fork Poplar Creek, oak ridge, Tennessee, USA. *Environmental Science: Processes & Impacts*, 20(4), 686–707. <https://doi.org/10.1039/c7em00538e>

Demers, J. D., Blum, J. D., & Zak, D. R. (2013). Mercury isotopes in a forested ecosystem: Implications for air-surface exchange dynamics and the global mercury cycle. *Global Biogeochemical Cycles*, 27, 222–238. <https://doi.org/10.1002/gbc.20021>

Demers, J. D., Sherman, L. S., Blum, J. D., Marsik, F. J., & Dvonch, J. T. (2015). Coupling atmospheric mercury isotope ratios and meteorology to identify sources of mercury impacting a coastal urban-industrial region near Pensacola, Florida, USA. *Global Biogeochemical Cycles*, 29, 1689–1705. <https://doi.org/10.1002/2015gb005146>

Donovan, P. M., Blum, J. D., Demers, J. D., Gu, B. H., Brooks, S. C., & Peryam, J. (2014). Identification of multiple mercury sources to stream sediments near oak ridge, TN, USA. *Environmental Science & Technology*, 48(7), 3666–3674. <https://doi.org/10.1021/es4046549>

Draxler, R. R., & Hess, G. D. Dec., 1997, revised(Sept., 2014). *Description of the HYSPLIT 4 Modeling System (NOAA Technical Memorandum ERL ARL-224)*. Silver Spring, MD: NOAA Air Resources Laboratory.

Drevnick, P. E., Engstrom, D. R., Driscoll, C. T., Swain, E. B., Balogh, S. J., Kamman, N. C., et al. (2012). Spatial and temporal patterns of mercury accumulation in lacustrine sediments across the Laurentian Great Lakes region. *Environmental Pollution*, 161, 252–260. <https://doi.org/10.1016/j.envpol.2011.05.025>

Druckenbrod, D. L., Neiman, F. D., Richardson, D. L., & Wheeler, D. (2018). Land-use legacies in forests at Jefferson's Monticello plantation. *Journal of Vegetation Science*, 29(2), 307–316. <https://doi.org/10.1111/jvs.12599>

Eagles-Smith, C. A., Nelson, S. J., Willacker Jr., J. J., Flanagan, C. M., & Krabbenhoft, D. P. (2016). Dragonfly mercury project—A citizen science driven approach to linking surface-water chemistry and landscape characteristics to biosentinels on a national scale. In: U.S. Geological Survey.

Engle, M. A., Gustin, M. S., Johnson, D. W., Murphy, J. F., Miller, W. W., Walker, R. F., et al. (2006). Mercury distribution in two Sierran forest and one desert sagebrush steppe ecosystems and the effects of fire. *Science of the Total Environment*, 367(1), 222–233. <https://doi.org/10.1016/h.scitotenv.2005.11.025>

Enrico, M., Le Roux, G., Heimbürger, L. E., Van Beek, P., Souhaut, M., Chmeleff, J., & Sonke, J. E. (2017). Holocene atmospheric mercury levels reconstructed from peat bog mercury stable isotopes. *Environmental Science & Technology*, 51(11), 5899–5906. <https://doi.org/10.1021/acs.est.6b05804>

Enrico, M., Roux, G. L., Maruscak, N., Heimbürger, L. E., Claustres, A., Fu, X., et al. (2016). Atmospheric mercury transfer to peat bogs dominated by gaseous elemental mercury dry deposition. *Environmental Science & Technology*, 50(5), 2405–2412. <https://doi.org/10.1021/acs.est.5b06058>

Frelich, L. E., Bockheim, J. G., & Leide, J. E. (1989). Historical trends in tree-ring growth and chemistry across an air-quality gradient in Wisconsin. *Canadian Journal of Forest Research-Revue Canadienne De Recherche Forestiere*, 19(1), 113–121. <https://doi.org/10.1139/x89-015>

Friedli, H. R., Radke, L. F., Lu, J. Y., Banic, C. M., Leitch, W. R., & MacPherson, J. I. (2003). Mercury emissions from burning of biomass from temperate north American forests: Laboratory and airborne measurements. *Atmospheric Environment*, 37(2), 253–267. [https://doi.org/10.1016/s1352-2310\(02\)00819-1](https://doi.org/10.1016/s1352-2310(02)00819-1)

Fu, X. W., Heimbürger, L. E., & Sonke, J. E. (2014). Collection of atmospheric gaseous mercury for stable isotope analysis using iodine- and chlorine-impregnated activated carbon traps. *Journal of Analytical Atomic Spectrometry*, 29(5), 841–852. <https://doi.org/10.1039/c3ja50356a>

Fu, X. W., Maruscak, N., Wang, X., Gheusi, F., & Sonke, J. E. (2016). Isotopic composition of gaseous elemental mercury in the free troposphere of the pic Du Midi observatory, France. *Environmental Science & Technology*, 50(11), 5641–5650. <https://doi.org/10.1021/acs.est.6b00033>

Gbor, P. K., Wen, D. Y., Meng, F., Yang, F. Q., & Sloan, J. J. (2007). Modeling of mercury emission, transport and deposition in North America. *Atmospheric Environment*, 41(6), 1135–1149. <https://doi.org/10.1016/j.atmosenv.2006.10.005>

Gratz, L. E., Keeler, G. J., Blum, J. D., & Sherman, L. S. (2010). Isotopic composition and fractionation of mercury in Great Lakes precipitation and ambient air. *Environmental Science & Technology*, 44(20), 7764–7770. <https://doi.org/10.1021/es100383w>

Gravatt, G. F. (1949). Chestnut blight in Asia and North America. *Unasylva*, 3, 2–7.

Gray, J. E., Pribil, M. J., Van Metre, P. C., Borrok, D. M., & Thapalia, A. (2013). Identification of contamination in a lake sediment core using hg and Pb isotopic compositions, Lake Ballinger, Washington, USA. *Applied Geochemistry*, 29, 1–12. <https://doi.org/10.1016/j.apgeochem.2012.12.001>

Gray, J. E., Van Metre, P. C., Pribil, M. J., & Horowitz, A. J. (2015). Tracing historical trends of hg in the Mississippi River using hg concentrations and hg isotopic compositions in a Lake sediment core, Lake Whittington, Mississippi, USA. *Chemical Geology*, 395, 80–87. <https://doi.org/10.1016/j.chemgeo.2014.12.005>

Guédron, S., Amouroux, D., Sabatier, P., Desplanque, C., Develle, A. L., Barre, J., et al. (2016). A hundred year record of industrial and urban development in French Alps combining hg accumulation rates and isotope composition in sediment archives from Lake Luitel. *Chemical Geology*, 431, 10–19. <https://doi.org/10.1016/j.chemgeo.2016.03.016>

Gunda, T., & Scanlon, T. M. (2013). Topographical influences on the spatial distribution of soil mercury at the catchment scale. *Water, Air, and Soil Pollution*, 224(4), 1–13. <https://doi.org/10.1007/s11270-013-1511-7>

Heyvaert, A. C., Reuter, J. E., Slotton, D. G., & Goldman, C. R. (2000). Paleolimnological reconstruction of historical atmospheric lead and mercury deposition at Lake Tahoe, California-Nevada. *Environmental Science & Technology*, 34(17), 3588–3597. <https://doi.org/10.1021/es991309p>

Hojdová, M., Navrátil, T., Rohovec, J., Žák, K., Vaněk, A., Chrastný, V., et al. (2011). Changes in mercury deposition in a mining and smelting region as recorded in tree rings. *Water, Air, and Soil Pollution*, 216(1–4), 73–82. <https://doi.org/10.1007/s11270-010-0515-9>

Holmes, R. L. (1983). Computer-assisted quality control in tree-ring dating and measurement. *Tree-Ring Bulletin*, 44, 69–75.

Horowitz, H. M., Jacob, D. J., Amos, H. M., Streets, D. G., & Sunderland, E. M. (2014). Historical mercury releases from commercial products: Global environmental implications. *Environmental Science & Technology*, 48(17), 10,242–10,250. <https://doi.org/10.1021/es501337j>

Jiskra, M., Sonke, J. E., Obrist, D., Bieser, J., Ebinghaus, R., Myhre, C. L., et al. (2018). A vegetation control on seasonal variations in global atmospheric mercury concentrations. *Nature Geoscience*, 11(4), 244–250. <https://doi.org/10.1038/s41561-018-0078-8>

Jung, R., & Ahn, Y. S. (2017). Distribution of mercury concentrations in tree rings and surface soils adjacent to a phosphate fertilizer plant in southern Korea. *Bulletin of Environmental Contamination and Toxicology*, 99(2), 253–257. <https://doi.org/10.1007/s00128-017-2115-5>

Kolker, A., Engle, M. A., Orem, W. H., Bunnell, J. E., Lerch, H. E., Krabbenhoft, D. P., et al. (2008). Mercury, trace elements and organic constituents in atmospheric fine particulate matter, Shenandoah National Park, Virginia, USA: A combined approach to sampling and analysis. *Geostandards and Geoanalytical Research*, 32(3), 279–293. <https://doi.org/10.1111/j.1751-908X.2008.00913.x>

Kurz, A. Y., Blum, J. D., Washburn, S. J., & Baskaran, M. (2019). Changes in the mercury isotopic composition of sediments from a remote alpine lake in Wyoming, USA. *Science of the Total Environment*, 669, 973–982. <https://doi.org/10.1016/j.scitotenv.2019.03.165>

Lamborg, C. H., Fitzgerald, W. F., Damman, A. W. H., Benoit, J. M., Balcom, P. H., & Engstrom, D. R. (2002). Modern and historic atmospheric mercury fluxes in both hemispheres: Global and regional mercury cycling implications. *Global Biogeochemical Cycles*, 16(4), 1104. <https://doi.org/10.1029/2001gb001847>

Landers, D. H., Simonich, S. M., Jaffe, D., Geiser, L., Campbell, D. H., Schwindt, A., et al. (2010). The Western airborne contaminant assessment project (WACAP): An interdisciplinary evaluation of the impacts of airborne contaminants in Western US National Parks. *Environmental Science & Technology*, 44(3), 855–859. <https://doi.org/10.1021/es901866e>

Lauretta, D. S., Klaue, B., Blum, J. D., & Buseck, P. R. (2001). Mercury abundances and isotopic compositions in the Murchison (CM) and Allende (CV) carbonaceous chondrites. *Geochimica et Cosmochimica Acta*, 65(16), 2807–2818. [https://doi.org/10.1016/s0016-7037\(01\)00630-5](https://doi.org/10.1016/s0016-7037(01)00630-5)

Liu, H. W., Shao, J. J., Yu, B., Liang, Y., Duo, B., Fu, J. J., et al. (2019). Mercury isotopic compositions of mosses, conifer needles, and surface soils: Implications for mercury distribution and sources in Shergyla Mountain, Tibetan plateau. *Ecotoxicology and Environmental Safety*, 172, 225–231. <https://doi.org/10.1016/j.ecoenv.2019.01.082>

Ma, J., Hintelmann, H., Kirk, J. L., & Muir, D. C. G. (2013). Mercury concentrations and mercury isotope composition in lake sediment cores from the vicinity of a metal smelting facility in Flin Flon, Manitoba. *Chemical Geology*, 336, 96–102. <https://doi.org/10.1016/j.chemgeo.2012.10.037>

Maillard, F., Girardclos, O., Assad, M., Zappelini, C., Mena, J. M. P., Yung, L., et al. (2016). Dendrochemical assessment of mercury releases from a pond and dredged-sediment landfill impacted by a chlor-alkali plant. *Environmental Research*, 148, 122–126. <https://doi.org/10.1016/j.envres.2016.03.034>

National Oceanic and Atmospheric Administration (NOAA), (2016). National centers for environmental information, climate at a glance: U.S. time series, palmer drought severity index (PDSI). In: National Climate Data Center, NOAA.

Navratil, T., Novakova, T., Shanley, J. B., Rohovec, J., Matouskova, S., Vankova, M., & Norton, S. A. (2018). Larch tree rings as a tool for reconstructing 20th century central European atmospheric mercury trends. *Environmental Science & Technology*, 52(19), 11,060–11,068. <https://doi.org/10.1021/acs.est.8b02117>

Navratil, T., Simecek, M., Shanley, J. B., Rohovec, J., Hojdrova, M., & Houska, J. (2017). The history of mercury pollution near the Spolana chlor-alkali plant (Neratovice, Czech Republic) as recorded by Scots pine tree rings and other bioindicators. *Science of the Total Environment*, 586, 1182–1192. <https://doi.org/10.1016/j.scitotenv.2017.02.112>

Nippert, J. B., Duursma, R. A., & Marshall, J. D. (2004). Seasonal variation in photosynthetic capacity of montane conifers. *Functional Ecology*, 18(6), 876–886. <https://doi.org/10.1111/j.0269-8463.2004.00909.x>

Obrist, D., Johnson, D. W., & Edmonds, R. L. (2012). Effects of vegetation type on mercury concentrations and pools in two adjacent coniferous and deciduous forests. *Journal of Plant Nutrition and Soil Science*, 175(1), 68–77. <https://doi.org/10.1002/jpln.201000415>

Odabasi, M., Tolunay, D., Kara, M., Falay, E. O., Tuna, G., Altıok, H., et al. (2016). Investigation of spatial and historical variations of air pollution around an industrial region using trace and macro elements in tree components. *Science of the Total Environment*, 550, 1010–1021. <https://doi.org/10.1016/j.scitotenv.2016.01.197>

Olson, C. L., Jiskra, M., Sonke, J. E., & Obrist, D. (2019). Mercury in tundra vegetation of Alaska: Spatial and temporal dynamics and stable isotope patterns. *Science of the Total Environment*, 660, 1502–1512. <https://doi.org/10.1016/j.scitotenv.2019.01.058>

Pacyna, J. M., Travnikov, O., Simone, F. D., Hedgecock, I. M., Sundseth, K., Pacyna, E. G., et al. (2016). Current and future levels of mercury atmospheric pollution on a global scale. *Atmospheric Chemistry and Physics*, 16(19), 12,495–12,511. <https://doi.org/10.5194/acp-16-12495-2016>

Peckham, M. A., Gustin, M. S., & Weisberg, P. J. (2019). Assessment of the suitability of tree rings as archives of global and regional atmospheric mercury pollution. *Environmental Science & Technology*, 53(7), 3663–3671. <https://doi.org/10.1021/acs.est.8b06786>

Pirrone, N., Allegrini, I., Keeler, G. J., Nriagu, J. O., Rossmann, R., & Robbins, J. A. (1998). Historical atmospheric mercury emissions and depositions in North America compared to mercury accumulations in sedimentary records. *Atmospheric Environment*, 32(5), 929–940. [https://doi.org/10.1016/s1352-2310\(97\)00353-1](https://doi.org/10.1016/s1352-2310(97)00353-1)

Riscassi, A. L., & Scanlon, T. M. (2011). Controls on stream water dissolved mercury in three mid-Appalachian forested headwater catchments. *Water Resources Research*, 47, W12512. <https://doi.org/10.1029/2011wr010977>

Riscassi, A. L., & Scanlon, T. M. (2013). Particulate and dissolved mercury export in streamwater within three mid-Appalachian forested watersheds in the US. *Journal of Hydrology*, 501, 92–100. <https://doi.org/10.1016/j.jhydrol.2013.07.041>

Risch, M. R., DeWild, J. F., Gay, D. A., Zhang, L., Boyer, E. W., & Krabbenhoft, D. P. (2017). Atmospheric mercury deposition to forests in the eastern USA. *Environmental Pollution*, 228, 8–18. <https://doi.org/10.1016/j.envpol.2017.05.004>

Rutter, A. P., Schauer, J. J., Shafer, M. M., Creswell, J. E., Olson, M. R., Robinson, M., et al. (2011). Dry deposition of gaseous elemental mercury to plants and soils using mercury stable isotopes in a controlled environment. *Atmospheric Environment*, 45(4), 848–855. <https://doi.org/10.1016/j.atmosenv.2010.11.025>

Schuster, P. F., Krabbenhoft, D. P., Naftz, D. L., Cecil, L. D., Olson, M. L., Dewild, J. F., et al. (2002). Atmospheric mercury deposition during the last 270 years: A glacial ice core record of natural and anthropogenic sources. *Environmental Science & Technology*, 36(11), 2303–2310. <https://doi.org/10.1021/es0157503> ISSN 0013-936X

Siwik, E. I. H., Campbell, L. M., & Mierle, G. (2010). Distribution and trends of mercury in deciduous tree cores. *Environmental Pollution*, 158(6), 2067–2073. <https://doi.org/10.1016/j.envpol.2010.03.002>

Smith, C. N., Kesler, S. E., Blum, J. D., & Ryuba, J. J. (2008). Isotope geochemistry of mercury in source rocks, mineral deposits and spring deposits of the California coast ranges, USA. *Earth and Planetary Science Letters*, 269(3–4), 398–406. <https://doi.org/10.1016/j.epsl.2008.02.029>

Speer, J. H. (2010). *Fundamentals of Tree-Ring Research*. Tucson: University of Arizona Press.

Stamenkovic, J., & Gustin, M. S. (2009). Nonstomatal versus stomatal uptake of atmospheric mercury. *Environmental Science & Technology*, 43(5), 1367–1372. <https://doi.org/10.1021/es801583a>

Sun, G., Sommar, J., Feng, X., Lin, C. J., Ge, M., Wang, W., et al. (2016). Mass-dependent and -independent fractionation of mercury isotope during gas-phase oxidation of elemental mercury vapor by atomic Cl and Br. *Environmental Science & Technology*, 50(17), 9232–9241. <https://doi.org/10.1021/acs.est.6b01668>

Sun, R., Streets, D. G., Horowitz, H. M., Amos, H. M., Liu, G., Perrot, V., et al. (2016). Historical (1850–2010) mercury stable isotope inventory from anthropogenic sources to the atmosphere. *Elementa—Science of the Anthropocene*, 4, 1, 000091–15. <https://doi.org/10.12952/journal.elementa.000091>

Sun, R. Y. (2019). Mercury stable isotope fractionation during coal combustion in coal-fired boilers: Reconciling atmospheric hg isotope observations with hg isotope fractionation theory. *Bulletin of Environmental Contamination and Toxicology*, 102(5), 657–664. <https://doi.org/10.1007/s00128-018-2531-1>

Sunderland, E. M., Cohen, M. D., Selin, N. E., & Chmura, G. L. (2008). Reconciling models and measurements to assess trends in atmospheric mercury deposition. *Environmental Pollution*, 156(2), 526–535. <https://doi.org/10.1016/j.envpol.2008.01.021>

Temme, C., Blanchard, P., Steffen, A., Banic, C., Beauchamp, S., Poissant, L., et al. (2007). Trend, seasonal and multivariate analysis study of total gaseous mercury data from the Canadian atmospheric mercury measurement network (CAMNet). *Atmospheric Environment*, 41(26), 5423–5441. <https://doi.org/10.1016/j.atmosenv.2007.02.021>

United Nations Environmental Program (UNEP) (2013). *Global Mercury Assessment 2013: Sources, Emissions, Releases and Environmental Transport*. Geneva, Switzerland: UNEP Chemicals Branch.

United States Bureau of the Census (1949). Historical statistics of the United States 1789–1945. Washington, D.C.

United States Environmental Protection Agency (U.S. EPA) (2002). Method 1631 revision E: Mercury in water by oxidation, purge and trap, and cold vapor atomic fluorescence spectrometry.

United States Energy Information Administration (US EIA) (2012). *Annual Energy Review, 2011*. Washington, D.C: U.S. Energy Information Administration Office of Energy Statistics. U.S. Department of Energy.

URS Corporation (2015). *Comprehensive facility investigation report (RFI), former DuPont Waynesboro plant, Waynesboro, Virginia*. Conshohocken, PA: URS Corporation.

Washburn, S. J., Blum, J. D., Demers, J. D., Kurz, A. Y., & Landis, R. C. (2017). Isotopic characterization of mercury downstream of historic industrial contamination in the South River, Virginia. *Environmental Science & Technology*, 51(19), 10,965–10,973. <https://doi.org/10.1021/acs.est.7b02577>

Washburn, S. J., Blum, J. D., Kurz, A. Y., & Pizzuto, J. E. (2018). Spatial and temporal variation in the isotopic composition of mercury in the South River, VA. *Chemical Geology*, 494, 96–108. <https://doi.org/10.1016/j.chemgeo.2018.07.023>

Weigelt, A., Ebinghaus, R., Manning, A. J., Derwent, R. G., Simmonds, P. G., Spain, T. G., et al. (2015). Analysis and interpretation of 18 years of mercury observations since 1996 at Mace head, Ireland. *Atmospheric Environment*, 100, 85–93. <https://doi.org/10.1016/j.atmosenv.2014.10.050>

Witt, E. L., Kolka, R. K., Nater, E. A., & Wickman, T. R. (2009). Forest fire effects on mercury deposition in the boreal forest. *Environmental Science & Technology*, 43(6), 1776–1782. <https://doi.org/10.1021/es802634y>

Woerndle, G. E., Tsui, M. T. K., Sebestyen, S. D., Blum, J. D., Nie, X. P., & Kolka, R. K. (2018). New insights on ecosystem mercury cycling revealed by stable isotopes of mercury in water flowing from a headwater peatland catchment. *Environmental Science & Technology*, 52(4), 1854–1861. <https://doi.org/10.1021/acs.est.7b04449>

Wright, G., Woodward, C., Peri, L., Weisberg, P. J., & Gustin, M. S. (2014). Application of tree rings dendrochemistry for detecting historical trends in air hg concentrations across multiple scales. *Biogeochemistry*, 120(1–3), 149–162. <https://doi.org/10.1007/s10533-014-9987-9>

Yake, B. (2001). *The Use of Sediment Cores to Track Persistent Pollutants in Washington State*. Olympia, WA: Washington State Department of Ecology.

Yang, Y., Yanai, R. D., Driscoll, C. T., Montesdeoca, M., & Smith, K. T. (2018). Concentrations and content of mercury in bark, wood, and leaves in hardwoods and conifers in four forested sites in the northeastern USA. *PLoS ONE*, 13(4), e0196293. <https://doi.org/10.1371/journal.pone.0196293>

Yin, R., Feng, X., Wang, J., Li, P., Liu, J., Zhang, Y., et al. (2013). Mercury speciation and mercury isotope fractionation during ore roasting process and their implication to source identification of downstream sediment in the Wanshan mercury mining area, SW China. *Chemical Geology*, 336, 72–79. <https://doi.org/10.1016/j.chemgeo.2012.04.030>

York, D., Evensen, N. M., Martinez, M. L., & Delgado, J. D. (2004). Unified equations for the slope, intercept, and standard errors of the best straight line. *American Journal of Physics*, 72(3), 367–375. <https://doi.org/10.1119/1.1632486>

Young, J., Flemming, G., Townsend, P., & Fosser, J. (2006). *Vegetation of Shenandoah National Park Service* (Vol. 1.1, p. 103). Leetown Science Center, Kearneysville, WV: U.S. Geological Survey.

Yu, B., Fu, X., Yin, R., Zhang, H., Wang, X., Lin, C. J., et al. (2016). Isotopic composition of atmospheric mercury in China: New evidence for sources and transformation processes in air and in vegetation. *Environmental Science & Technology*, 50(17), 9262–9269. <https://doi.org/10.1021/acs.est.6b01782>

Zheng, W., & Hintemann, H. (2010). Isotope fractionation of mercury during its photochemical reduction by low-molecular-weight organic compounds. *The Journal of Physical Chemistry A*, 114(12), 4246–4253. <https://doi.org/10.1021/jp9111348>

Zheng, W., Oberst, D., Weis, D., & Bergquist, B. A. (2016). Mercury isotope compositions across north American forests. *Global Biogeochemical Cycles*, 30, 1475–1492. <https://doi.org/10.1002/2015gb005323>

### References From the Supporting Information

Lee, T. R., De Wekker, S. F. J., Andrews, A. E., Kofler, J., & Williams, J. (2012). Carbon dioxide variability during cold front passages and fair weather days at a forested mountaintop site. *Atmospheric Environment*, 46, 405–416. <https://doi.org/10.1016/j.atmosenv.2011.09.068>

Lee, T. R., De Wekker, S. F. J., Pal, S., Andrews, A. E., & Kofler, J. (2015). Meteorological controls on the diurnal variability of carbon monoxide mixing ratio at a mountaintop monitoring site in the Appalachian Mountains. *Tellus Series B: Chemical and Physical Meteorology*, 67(1), 25659. <https://doi.org/10.3402/tellusb.v67.25659>